Control of the nanostructure of MgO–Y2O3 composite ceramics using two-step sintering for high temperature mid infrared window applications

Nathan Brard, Johan Petit, Nicolas Emery, Nicolas Horezan, Stéphane Bach

Control of the nanostructure of MgO-Y_2O_3 composite ceramics using two-step sintering for high temperature mid infrared window applications

Nathan BRARD[a, b], Johan PETIT[a], Nicolas EMERY[b], Nicolas HOREZAN[a], Stéphane BACH[b,c]

[a] DMAS, ONERA, Université Paris Saclay F-92322 Châtillon - France
[b] ICMPE, CNRS, UMR 7182, 2 Rue Henri Dunant, 94320 Thiais, France
[c] Université Paris Saclay - Evry, Dept Chimie, Bd F. Mitterrand, 91000 Evry, France

Keywords

Y_2O_3-MgO nanocomposites, SPS, two-step sintering, sol-gel synthesis, IR transparent ceramic

Abstract

Transparent Y_2O_3-MgO nanocomposite ceramic has been processed for mid-IR window applications. The powder was synthesized by a sol-gel route. The final temperature of this process has an impact on the crystallite size and crystallization ratio. A homogeneous powder with around 10 nm crystallite size was made with a final temperature of 600°C. The powder was then sintered by the SPS technique performing a two-step sintering process at 1200°C/50 MPa instead of a conventional bearing. A fully dense ceramic (>99%) with an average grain diameter of 150 nm (compared to 350 nm with one-stage sintering) was obtained. After HIP at 400 MPa and annealing in air for 100 h post-treatments, the IR transmittance in the 3-5 µm wavelength range exceeds 80% for a thickness of 1 mm. Transparency loss at 5 µm is less than 10% at 1000°C, which is more suitable for the IR's band II than materials such as sapphire, spinel or AlON.

1) Introduction

Transparent ceramics are materials of choice for high temperature infrared (IR) windows [1], [2]. Those windows are particularly used for aerospace applications. In this field, one of the challenges is to maintain sufficient IR transparency between 3 and 5 µm wavelength (band II) even at high temperature (1000°C) in atmospheric conditions. Indeed, these compounds show a degradation of their optical properties (transparency and emissivity) with the increase of temperature in the infrared because of the phonons' absorption [3], [4]. Alumina, AlON and spinel-type ceramics have been developed for 3-5 µm band applications because of their transparency up to 6 µm [4]. Nevertheless, at high temperature, strong absorptions occur below 5 µm and impact band II transparency limiting their use [3], [5], [6]. Thus, one way to go further is to find materials with a transparency beyond 6 µm to limit temperature impact on the 3-5 µm band transparency.

MgO and Y_2O_3 are transparent up to 9 µm but their thermomechanical resistances are quite weak when tested separately to be used in a harsh environment [4]. However, many studies have combined these compounds into MgO-Y_2O_3 nanocomposite ceramics [7]–[10]. They proved that the nanostructure, assisted by the slowing down of granular growth due to their immiscibility [11], [12], have permitted to keep a good IR transparency and increases its mechanical resistance. Thus, to reach such properties, the porosity ratio must be close to zero and the microstructure must be as homogeneous as possible. In addition, the average grain size must stay as small as possible (< 200 nm) due to the difference between MgO and Y_2O_3 refractive index values which leads to scattering at grain boundaries [13]–[15] and to improve its mechanical properties [16].

Several authors have developed dense MgO-Y_2O_3 nanocomposite ceramics with a homogeneous microstructure. Many powder synthesis routes have been reported: the mains are flame spray pyrolysis [10], colloidal dispersion of commercial powders [17], thermal decomposition [18] and sol-gel method [19]. For sintering, natural sintering [8], hot pressing [12], [20] or Spark Plasma Sintering (SPS) [21], [22] have been considered before an air annealing and/or a Hot Isostatic Pressing (HIP) post treatments. These materials exhibit very interesting optical properties (3-5 µm band transmission higher than 80% for a thickness of 1-2 mm) even up to 500°C (transparency higher than 76% and almost unchanged at 500°C for a thickness of 1mm) [23]. By reducing the grain size to less than 100 nm, transparency in the visible is even considered [24]. In addition, the composite has better mechanical properties (bending strength, thermal shock resistance) than pure MgO and Y_2O_3 [9].

Through this study, Pechini's esterification sol-gel route was chosen in order to process the nanocomposite powder [25], [26]. This route is based on the formation of chelate between magnesium and yttrium nitrate previously solubilized in deionized water with citric acid. The two cations are chelated and in a second step, with the presence of ethylene glycol, the chelates are cross-linked to create a gel through polyesterification. A powder is then obtained by oxidation when increasing the temperature. The sol-gel route was naturally chosen get a homogeneous nanometric powder dispersed in the polymeric network with an uniform distribution of cations. We have investigated the sol-gel synthesis by varying the final treatment temperature and the impact of the average crystallite size on the microstructure. We have carried out a novel two-step sintering by the SPS technique to densify our ceramics. The SPS has the advantage of being able to sinter quickly under pressure and a two-step sintering technique profile favors the densification over granular growth [27]–[29]. Indeed, Ma et al. have successfully used a two-step hot pressing to improve density and transmission of a MgO-Y_2O_3 nanocomposite with limited grain growth [30]. They reached a higher temperature before performing a decreasing to a long step of one hour at a lower temperature. In our work, a rapid cooling was performed after reaching the sintering temperature and just before an additional short 10 min step at the same temperature. To our knowledge, such a sintering profile has not been done yet on that compound. This whole process was followed by a post HIP treatment at 400 MPa. Finally, the optical transparency of these composite materials was determined up to 1000°C.

2) Material and methods

2.1) Synthesis of MgO-Y_2O_3 nanocomposite powder

MgO-Y_2O_3 nanocomposite powders were synthetized using the Pechini's process, with a composition leading to a volume ratio between the two oxides of 50:50 in the final sintered samples. An aqueous solution was prepared using magnesium nitrate hexahydrate ($Mg(NO_3)_2{\cdot}6H_2O$, 99.5%), yttrium nitrate hexahydrate ($Y(NO_3)_3{\cdot}6H_2O$, 99.5%), citric acid monohydrate ($C_6H_8O_7{\cdot}H_2O$, 99.5%) and ethylene glycol ($C_2H_6O_2$, 99%). The molar ratio of citric acid on ethylene glycol was settled to 3.39 and the molar ratio of citric acid on metal nitrates to 0.45, according to the proportions used by Xu et al. [31]. Both magnesium and yttrium nitrates were previously solubilized in deionized water. As a second step, an alumina crucible was filled with the solution. Batches of 10 g, for the first tests at different temperature, and then 50 g of powders were synthesized and heat treated in 0.5 L and 2.5 L alumina crucibles respectively. Crucibles were placed in an oven at 200°C for 3 h to evaporate the water of the solution. Once the gel was formed, crucibles were put in a muffle furnace preheated at 200°C. Afterwards, the furnace was heated at a rate of 100°C/h from 200°C to a

temperature included between 600°C and 1200°C, and kept 2 h at the chosen temperature to obtain the powder (FIG 1). After this thermal treatment, the powder was crushed in a glass mortar and sieved at 50 µm. The MgO-Y_2O_3 nanocomposite powders were finally dried in an oven at 150°C and stored into a desiccator.

FIG 1. MgO-Y2O3 nanocomposite powder (10g) obtained after the 600-1200°C heat treatment (thermal sol-gel process). Inner diameter of the crucible = 90mm. **(1-column fitting image)**

2.2) Sintering

These powders were sintered using our SPS facility with unpulsed direct current. ONERA's SPS can deliver currents up to 40 kA and a force up to 250 t, allowing samples of 20 to 300 mm in diameter to be sintered. A graphite die was filled in with powder to make pellets with a 30 mm diameter and a 3 mm thickness (after sintering). Electric and thermal contacts between rams, powder and mold were provided by two layers of 0.25 mm thick graphite paper. For the sintering treatments, two thermal profiles were used with a maximum temperature of 1200°C. In both of them, ramps of 200°C/min under 50 MPa were applied to reach 1200°C with a pre-sintering dwell of 5 min at 850°C during which the pressure is increased from 10 MPa to 50 MPa (FIG 2). The first thermal profile was composed of a simple step of 10 min at 1200°C. The second thermal profile was composed of two steps: first, the temperature was raised up to the sintering temperature (1200°C) and at this temperature the power was stopped and the pressure was suddenly released to let the sample cool down naturally to room temperature. This step is a kind of “quenching”. A second step is then added with a classical dwell of 10 min at 1200°C (FIG 2). For the rest of this study, the two profiles will be referred as “one-step” or “two-step” process. In order to better interpret the difference of the profile, a sample was analyzed just after the first heating of the two step profile. Furthermore, temperatures were both measured by an optical pyrometer focusing on a hole in the side of the die and a thermocouple measuring the temperature through one of the two pistons at 4 mm from the center of the sample. The temperature process was controlled by the thermocouple temperature.

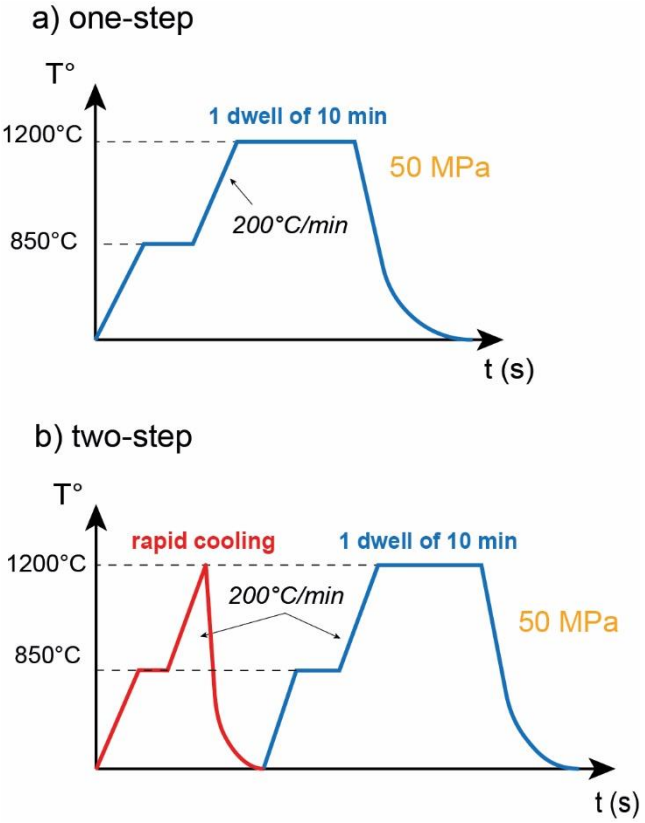

FIG 2. Thermal profiles for the SPS process: a) with "one step" b) with "two step". **(1-column fitting image)**

Sintered samples were then Hot Isostatically Pressed (HIP) at 1200°C under 400 MPa for 2 h. Then, samples were air annealed in a muffle furnace for 20 to 100 h at 1000°C. Finally, a polishing down to 1/4 µm was carried out prior to their characterizations.

2.3) Characterization

Thermogravimetric analysis of the sol-gel synthesis and pure magnesium and yttrium nitrates hexahydrated oxidation were performed from distinct analyses under air using alumina crucibles. The MgO-Y_2O_3 nanocomposite powder was observed by transmission electron microscope (TEM) and analyzed by X-ray diffraction (XRD) using a diffractometer with a Co Kα source. GSAS-EXPGUI package [32], [33] was employed to analyze the diffraction patterns with the Rietveld method to determine the ratio of crystallized MgO and Y_2O_3 of the total crystalline phases and the average crystallites sizes using the Scherrer formula. For sintered samples, their microstructure was observed using a scanning electron microscope (SEM). Images were collected on polished slices of sintered samples and the average grain size was measured using the intercept method on the SEM pictures with a coefficient of 1.56 [34]. Moreover, the porosity ratio was measured using the Archimedes method, assuming a density of 4.293 g/cm^3 for the 50:50 vol% composite. The accuracy of that method is around 1%. Optical transmission in the near and the mid infrared of the MgO-Y_2O_3 nanocomposite samples were performed using a Fourier Transform IR spectrophotometer. Transmission curves were measured on samples of a given thickness and then re-calculated to correspond to a thickness of 1 mm to facilitate the comparison between samples. For this purpose, the attenuation coefficient, as a function of wavelength, $\alpha(\lambda)$ (cm^{-1}), is calculated from equation (1) with taking into account multiple reflections on the surfaces [13], [14]:

$$\alpha(\lambda) = \frac{1}{l}\ln\left[\frac{2n(\lambda)}{RIT(1+n(\lambda)^2)}\right] \quad (1)$$

Where RIT is the Real In line Transmission, l (cm) the thickness of the sample and $n(\lambda)$ is the refractive index of the sample at the wavelength λ. The average index between the two indices of MgO and Y_2O_3 at 4.85 µm, $n_{MgO-Y_2O_3} = 1.7321$, have been chosen from Harris et al. [9]. This results in 86 % for the theoretical transmittance limit, taking into account perfect diopter reflections. A special care should be taken when analyzing the graphs because this calculation can significantly amplify error below 15 % of transmission.

At last, the high-temperature transmission measurements were carried out using a specific IR scanning spectrophotometer assembled at ONERA. The sample is heated in a chamber at temperatures ranging from 20 to 1000°C. Measurements are made using a monochromator, a lock in amplifier, anti-reflected ZnSe optics, an IR lamp, a long-pass filter at 4.5 µm and a 77K cooled MCT detector.

3) Results and discussion

3.1) Powder synthesis, crystallite size and quality

The different steps of the sol-gel process were investigated by thermogravimetric analysis shown in the FIG 3. In the first plot (FIG 3a), a dried gel obtained just after the drying step at 200°C was analyzed. In the second graph (FIG 3b), two other thermogravimetric analyses were carried out using pure magnesium and yttrium nitrate powders separately. The graph shows the mass loss derivative to emphasize the results.

One can see on the FIG 3a that, below 250°C, the mass loss is mainly due to water evaporation from the solution and then from esterification. Then, organic compounds begin to be oxidized. Beyond 350°C, nitrates decompose. For temperatures above 800°C, most of the organic compounds and other volatiles are gone. The two most important mass losses at 360°C and 430°C are due to nitrate decompositions, in the form of NO_2, as it can be compared with the FIG 3b.

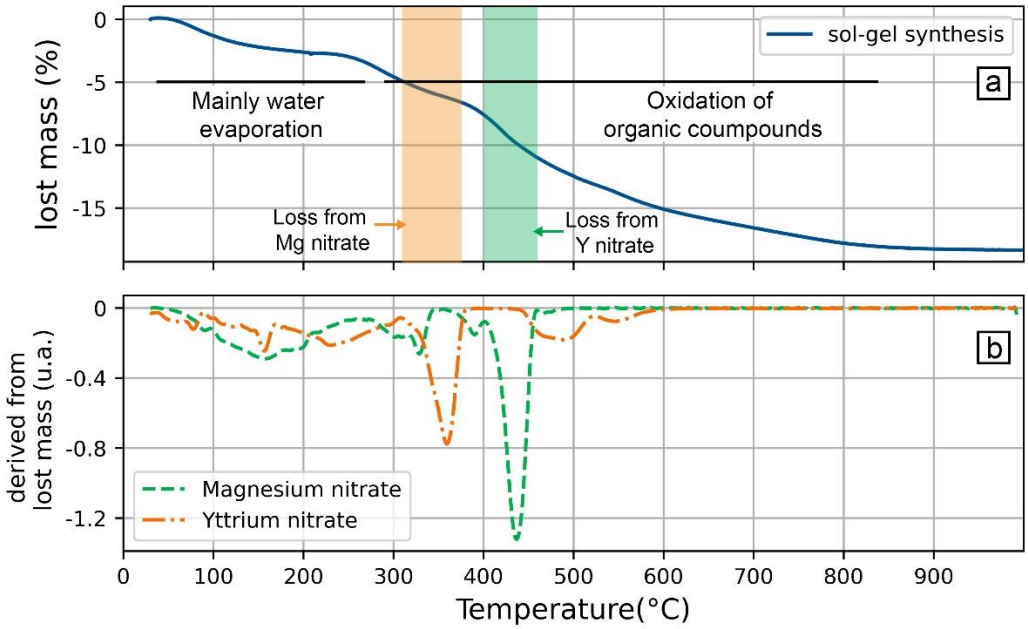

FIG 3. Thermogravimetric analysis (rise in 3°C per min). a: mass loss as a function of the temperature during sol-gel synthesis of a MgO-Y_2O_3 nanocomposite powder after a pre-treatment at 200°C during 2h. b: Derivatives from the mass loss as a function of the temperature of pure magnesium and yttrium nitrates hexahydrated obtained from distinct analyses. **(1.5-column fitting image)**

The FIG 4 shows an aggregate of the sol-gel powder after a thermal treatment at 800°C. The crystallite size appears to be well below 100 nm.

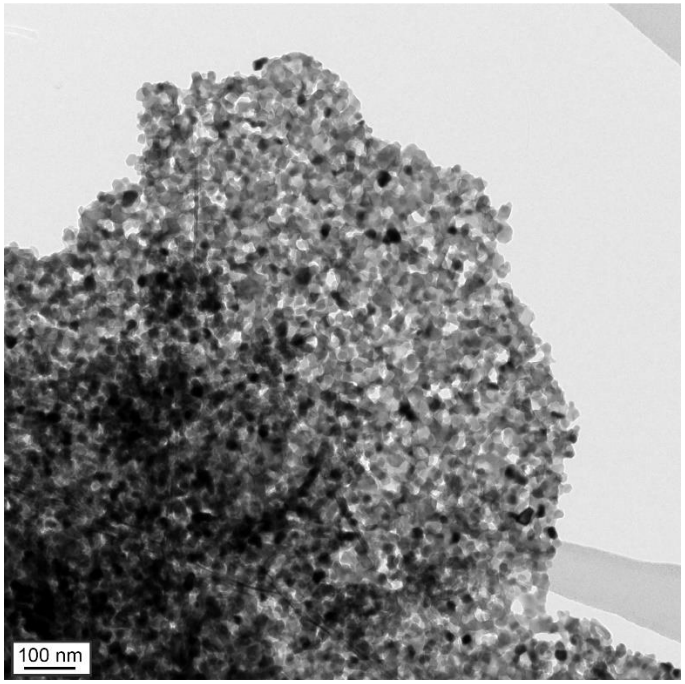

FIG 4. TEM images of the sol-gel powder synthetized at 800°C. **(1-column fitting image)**

The synthesis seems to be completed at 800°C. Increasing the temperature of the thermal treatment will affect the crystallinity of the powders. We tested treatments with a temperature between 600°C and 1200°C. XRD analyses confirm that for all the temperatures, both MgO and Y_2O_3 are present without any additional phase (FIG 5). The higher the temperature, the lower the full half maximum width of the diffraction peaks is, meaning an increasing average grain size. Then, Rietveld refinements were performed using the GSAS-EXPGUI software suite with a good correlation to the experimental curves (FIG 5). Relevant refined parameters are given in Table 1. It can be noted that lattice constants decrease with the increase of the synthesis temperature. According with the nanoparticles behaviors, the lattice parameter decreases as the crystallite size increases for nanometric sizes [35].

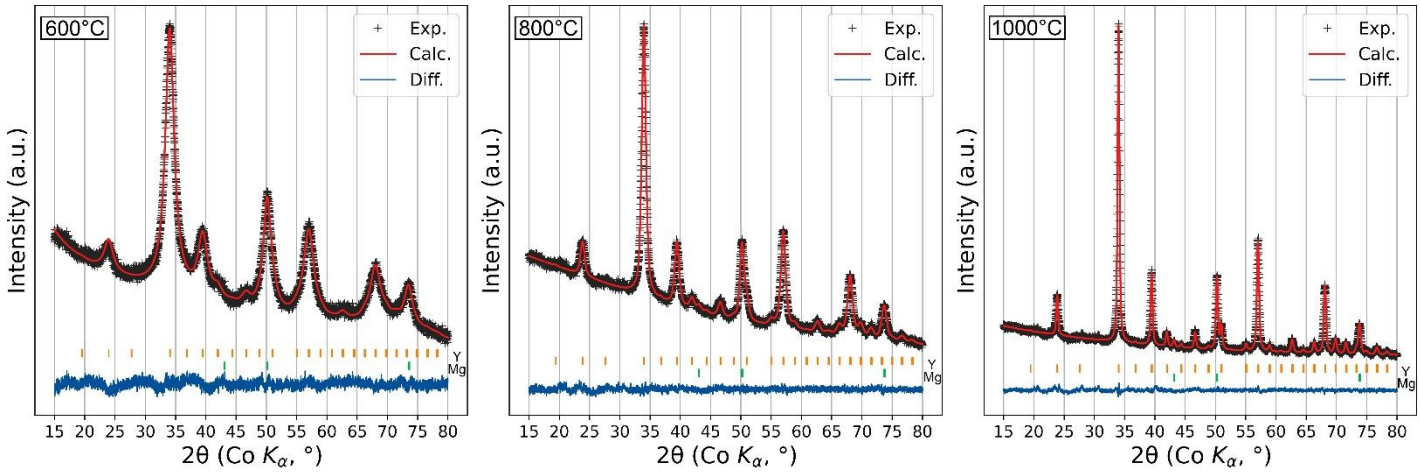

FIG 5. X-ray Diffraction on sol-gel powders synthesized with different final temperatures (λ_{cobalt}=1.7889 Å) in black cross. The peaks corresponding to the plane families of MgO (Mg) and Y_2O_3 (Y) are indicated by green and orange vertical lines below. The red solid lines represent the curves calculated by Rietveld refinement. The blue solid lines show the difference between the experimental curves and the calculated curves. **(2-column fitting image)**

Table 1. Relevant refined parameters and statistical index (chi², Rp and Rwp) from Rietveld refinement of MgO-Y_2O_3 nanocomposite powders synthesised at different temperatures. Standard deviation is given in brackets. MgO has a cubic crystal system (space group: Fm-3m) with a lattice constant of 4.217 Å [36]. Y_2O_3 has a cubic crystal system (space group: Ia-3) with a lattice constant of 10.604 Å [37].

Powder synthesis temperature (°C)	Lattice constant (Å)		Mass fraction of MgO (%)	Estimated crystallite sizes (nm)		Chi²	Rp (%)	Rwp (%)
	MgO	Y_2O_3		MgO	Y_2O_3			
600	4.238 (5)	10.64 (1)	55 (0.4)	7	5	1.799	1.19	1.49
700	4.225 (2)	10.617 (5)	46 (0.3)	18	12	1.632	1.12	1.41
800	4.220 (2)	10.607 (4)	45 (0.3)	24	18	1.522	1.11	1.40
900	4.217 (1)	10.605 (2)	44 (0.3)	32	29	1.841	1.11	1.40
1000	4.215 (1)	10.603 (2)	44 (0.3)	44	40	2.021	1.14	1.47
1200	4.214 (1)	10.600 (1)	42 (0.3)	77	71	2.677	1.27	1.69

Results from the treatment of the diffractograms by Rietveld refinement were undertaken to determine the mean grain size of crystallites inside the powders. They are presented in the FIG 6. First, the mean crystallite diameter of the powder increases logically with the temperature (FIG 6a). The average crystallite diameter goes from 10 nm at 600°C to about 70-80 nm for a temperature of 1200°C. Moreover, the FIG 6b shows the evolution of the crystalline phase ratio of MgO in the total crystalline phase (MgO + Y_2O_3) as a function of the final temperature treatment of the powder. It suggests that magnesia crystallizes at a lower temperature than yttria and the expected theoretical volume ratio (50/50) appears beyond 800/900°C. Below this temperature, a higher fraction of Y_2O_3 than MgO remains amorphous. However, it is expected that the yttria amorphous fraction will crystallize during the sintering process (around 1200°C), leading to a sintered sample without amorphous domains. In addition, keeping a small crystallite size by heating the powder at a lower temperature will have a positive impact on the final grain size after SPS treatments.

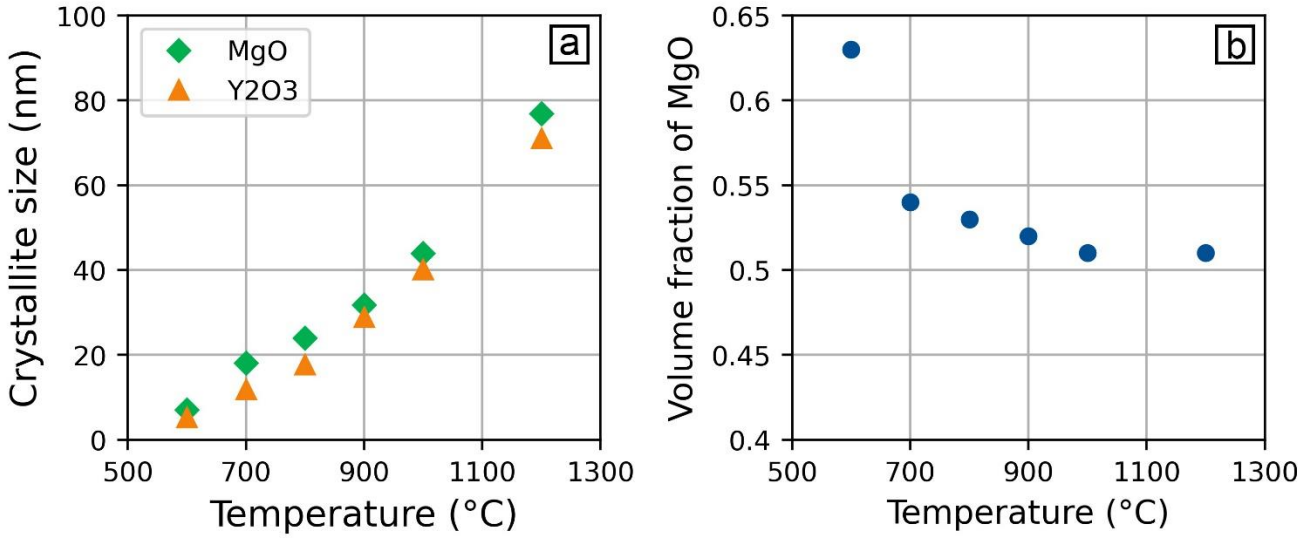

FIG 6. a: Crystallite size as a function of sol-gel final temperature treatment. b: Volume fraction of the MgO crystalline phase as a function of sol-gel final temperature treatment (calculated from the mass fraction obtained with Rietveld analysis). **(2-column fitting image)**

3.2) SPS Sintering and grain size

Several samples have been processed to study the impact of the crystallite size but also of the thermal treatment on the post-sintering microstructure. Table 2 summarizes the process parameters corresponding to the samples and gives the average grain diameters of each ceramic as well as their porosity ratio. Samples' microstructure by SEM micrographs are presented in FIG 7.

Table 2. Summary of the different MgO-Y_2O_3 nanocomposite samples processed in the present work. Mean grain size (intercept method with 1.56 ratio) and porosity ratio (Archimedes method) are given depending on the process parameters. Air annealing was processed at 1000°C and HIP at 1200°C under 400MPa.

Sample	Powder synthesis temperature (°C)	Sintering conditions	Post treatments	Mean grain size (nm)	Porosity ratio (%) *± 1%*
1A	600	One step	-	280	12
1B	700	One step	-	300	13
1C	800	One step	-	350	10
1D	1000	One step	-	410	9
2A	800	Two-step	-	150	< 1
2B	800	Intermediate two-step	-	100	10
2C	800	Two-step	Air annealing (20h)	180	< 1
2D	800	Two-step	HIP (2h)	220	< 1
2E	800	Two-step	HIP (2h) + Air annealing (20h)	230	< 1
2F	800	Two-step	HIP (2h) + Air annealing (100h)	240	< 1

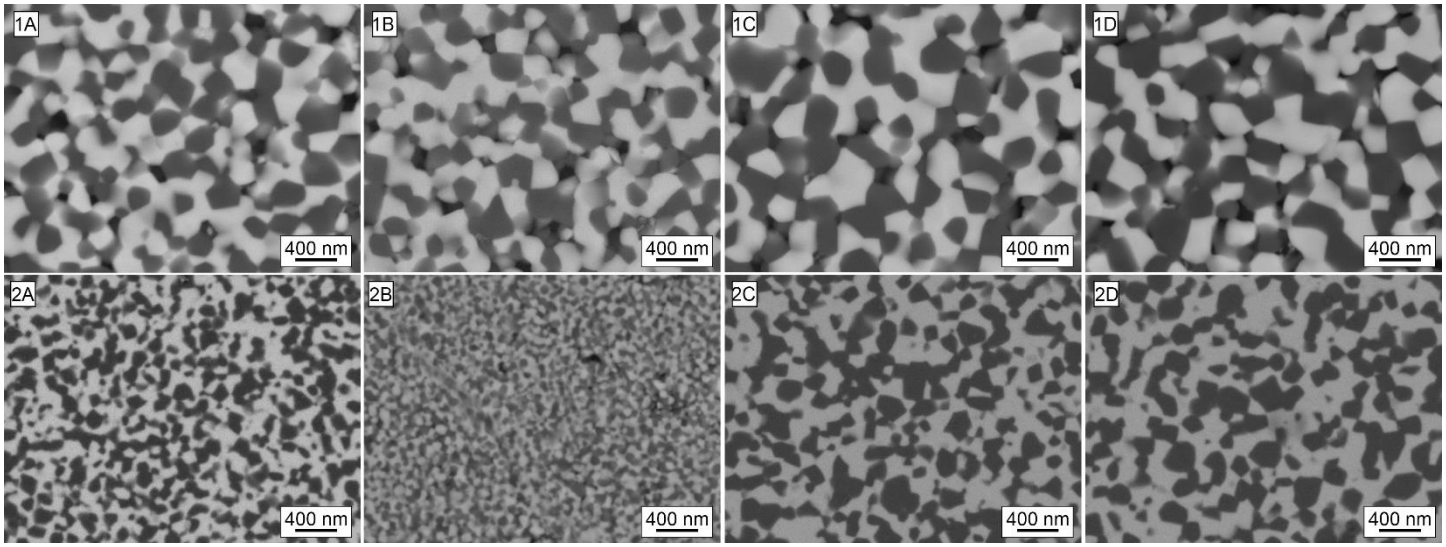

FIG 7. SEM pictures (BSE) showing the microstructures (light: yttria; dark: magnesia) of MgO-Y_2O_3 nanocomposite samples. On the first row, the samples were all one-step sintered with powders synthetized by sol-gel process at different temperatures. 1A: 600°C, 1B: 700°C, 1C: 800°C, 1D: 1000°C. On the second row, the samples were two-step sintered with the same powder synthetized at 800°C and then post treated. Sintering of the sample 2B was stopped after the rapid cooling. 2A and 2B: no post treatment, 2C: 20 h air annealing at 1000°C, 2D: HIP at 1200°C under 400 MPa during 2 h. **(2-column fitting image)**

On the one hand, a classical one-step sintering as presented in the experimental part was performed on the synthesized powders prepared at 600 to 1000°C by the sol-gel process. After a same sintering procedure, a finer microstructure is obtained for ceramic prepared from finer powder. An increase of about 100 nm of the average grain diameter is observed between the nanocomposite sintered from a powder prepared at 600°C (1A) and the ceramic obtained from powder prepared at 1000°C (1D). Nevertheless, the one-step sintering thermal profile is not efficient enough in terms of control of the grain size and improvement of the density. Indeed, in all these samples, the density remains around 90%, which is too low to expect a good IR transmission. The origin of this quite low density could be explained by the characteristics of the powder such as the morphology and distribution of aggregates. Xie et al. have highlighted the possible creation of porosity if a rapid moisture release occurs during sintering because the hydrophilicity of MgO-Y_2O_3 nanopowders [22]. In the present study, even with a powder treated above 1000°C (1D), the density is still quite low.

On the other hand, as presented in the experimental part, our novel two-step SPS sintering profile has been tested in order to improve the quality of the ceramic. The Table 2 sums up the characteristics of the two-step sintered samples from the powder treated at 800°C (2A). Post treated ceramics by air annealing at 1000°C for 20 h (2C), by HIP at 1200°C under 400 MPa for 2 h (2D) and by HIP (same conditions) followed by air annealing 20 h (2E) or 100 h (2F) are also shown. The sintering of the sample 2B was stopped in the intermediate stage, after the first rapid cooling and before the 10 min stage. As seen in the Table 2 the two-step SPS treatment allows

to keep the grain size twice as small as with the one-step profile and also to keep the porosity ratio below 1%. Adding post treatments makes the grain size grow but it stays below 250 nm.

So, the two-step sintering method as proposed in the present work is clearly an effective process to prepare MgO-Y_2O_3 nanocomposites with a high densification and a reduced grain size. The two-step profiles proposed by Chu et al. [27] or from Chen and Wang [28] are slightly different than ours and have also yielded good results in grain growth inhibition. They explain that the reduction of the driving force for grain growth could be obtained with the modification of the grain size distribution and the creation of a network of grain boundaries anchored by the relatively immobile three-grain junction lines, the four-grain junction points and so on. The energy required for the migration of these junctions is quite high and, at the second step, favours the diffusion along the grain boundaries limiting the grain growth. If a critical density is initially achieved in the first step, there are enough of those junctions throughout the sample to inhibit the migration of grain boundaries in the following phase [29], [38]. In this study, the intermediate sample (2B) has a porosity ratio of 10% which seems to be enough to avoid the grain growth during the second step. As the temperature in the second step is similar to the first one, the thermal history of this material (i.e., the sudden cooling at the beginning of the step) plays a significant role. The formation of a microstructure favouring diffusion at grain boundaries as described above could be promoted by the rapid cooling and the pressure release.

In addition, the two post-treatments are very important to improve the quality of our material. In the case of air annealing, the objective is to reduce mechanical stresses within the ceramic and to fill the oxygen vacancies formed during SPS sintering, which is a reducing environment. Otherwise, the HIP treatment increases the sample density as much as possible. As shown in the FIG 7 and Table 2, both processes (2C and 2D) slightly increase the grain size which still stays fine. Optimization of the annealing and HIP parameters will be done in further work.

3.3) Optical properties

The FT-IR spectrometer transmittance of the samples are given in the FIG 8. These curves are calculated from experimental curves to correspond to a 1 mm thick sample.

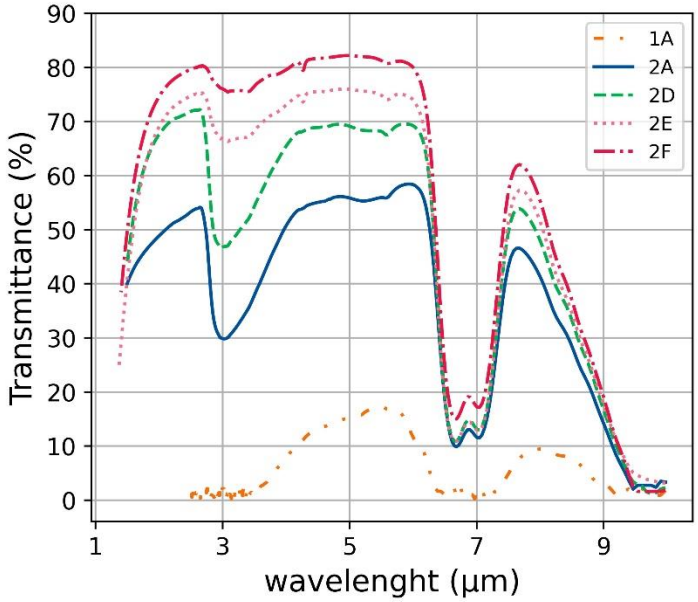

FIG 8. FT-IR transmittance of MgO-Y_2O_3 nanocomposite samples sintered in different ways (resumed inTable 2). These curves are calculated to correspond to a 1mm thick sample. **(1-column fitting image)**

Firstly, near and mid-infrared transmittance of 1C and 2A samples, sintered with the same powder, are compared. The transmittance of the two-step sintered sample, which has a finer and denser microstructure, is clearly higher than the one obtained with the one-step profile, which has a porosity ratio of almost 10%. Indeed, the transparency of the former reaches about 55% between 4 and 6 µm for a thickness of 1 mm whereas, for the latter, it stays below 20%. Nevertheless, two absorption bands can be observed: one around 3 µm is related to the remaining hydroxyled compounds. This band is particularly annoying because it affects the 3-5 µm band. The second absorption band around 7 µm would be caused by the stretching vibration of a carboxylate group because of carbon

contamination from the SPS or from the sol-gel process [39]. To improve the transparency, the results of several post-treatments are then presented in the FIG 8. The HIP at 400 MPa (1200°C, 2 h), which reduces the size and quantity of the pores, greatly improves the overall transparency of the sample 2D. In this case, the transparency for 1 mm thickness reached 70% at 5 µm. However, this process does not have an impact on the different absorption peaks. Subsequently, air annealing further improves the overall transparency of the samples 2E and 2F. It goes up to around 75% at 5 µm for a 20 hours treatment and exceeds 80% for a 100 hours treatment. Annealing also reduces significantly the absorption band around 3 µm. Unfortunately, the peak around 7 µm is not affected. Some authors showed that it is possible to make it disappear by using additives such as LiF in the powder [40]. However, this peak is not located between 3 and 5 µm wavelength and so does not really affects the potential applications in that range. However, we needed to check that the band does not move to the 3-5 µm range when the temperature increases.

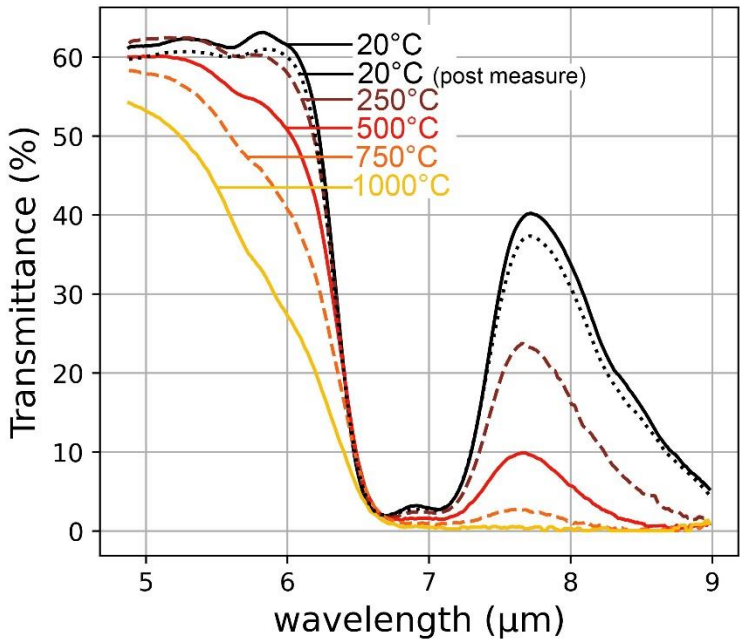

FIG 9. Infrared transmittance of a 2 mm thick MgO-Y2O3 nanocomposite sample from 20°C to 1000°C. The sample was sintered by SPS with a two-step sintering (1200°C, 50MPa, 200°C/min) followed by HIP (1200°C, 2h, 400MPa) and air annealing (1200°C, 100h). **(1-column fitting image)**

The FIG 9 presents the transparency of the MgO-Y_2O_3 nanocomposite sample 2F sintered by the two-step SPS profile followed by a HIP post-treatment (400 MPa, 1200°C, 2 h) and then air annealing (1000°C, 100 h) at temperatures up to 1000°C. In this figure, one can see that the overall transmittance is lower at room temperature than in FIG 8 (about 60% versus 80%). This is due to the 2 mm thickness and also because the detector in the high temperature transmission bench is located at a much longer distance from the sample than in the FTIR spectrometer (FIG 8). Nevertheless, when the temperature increases, the sample transmittance decreases gradually from the longer wavelength to the shorter wavelengths. This behaviour is related to multiphoton absorption. When the temperature increases, there is more energy and a higher probability for multiples phonon to absorb a photon, decreasing the transmittance [41]. Consequently, the material's emissivity also increases, which may have a strong impact on the signal to noise ratio measured by an IR detector according to the application [3], [4]. This is a well-known limit of the infrared windows at high temperatures. In the MgO-Y2O3 nanocomposite material, at 5µm, there is almost no effect up to 500°C and then it decreases very slowly. At 1000°C, the loss of transparency remains below 10%. After measurement at high temperature, another measurement was carried out à 20°C to verify that there is no irreversible modification of the sample quality. This measurement, presented in the FIG 9 too, shows a very slight loss of the transparency, surely due to partial reduction of the sample during the measurement in the graphite furnace. To conclude, compared to the other well-known materials whose optical properties at 5 µm temperature are summarized in the Table 3, those measurement confirm that losses in 3-5 µm band are less significant in MgO-Y_2O_3 that in sapphire for example. Furthermore, the absorption peak at 7 µm due to carbon pollution during the production process does not change in temperature and does not seem to be a problem.

Table 3. Transmittance at 5µm at low and high temperature for transparent ceramics.

Materials	Thickness	Transmittance at low temperature	Transmittance at High temperature	Refs
Sapphire (c-axis)	2 mm	75% (25°C)	61% (427°C) 43% (827°C)	[5]
AlON	2 mm	63% (25°C)	44% (500°C)	Calculated from [6]
Spinel	2 mm	78% (25°C)	66% (500°C)	Calculated from [6]
MgO-Y2O3 nanocomposite	1mm	86% (25°C)	83% (500°C)	[23]
MgO-Y2O3 nanocomposite	2 mm	61% (20°C)	60% (500°C) 53% (1000°C)	This work

4) Conclusion

Nanocomposite powders of magnesia and yttria with a volume ratio of 50:50 have been synthetized by a sol-gel route. By varying the temperature treatment in this process, it was possible to obtain grains of varying sizes and we observe different amorphous/crystalline phase ratio. With a synthesis at 1200°C, crystallites between 70 and 80 nm were obtained. By lowering the synthesis temperature to 600°C, the crystallite size is reduced to about 10 nm. Using powders produced at lower temperatures resulted in sintered materials with finer microstructures.

Next, a novel two-step profile was proposed for SPS sintering. The rapid cooling and the pressure release, seem to have to be taken into consideration in the formation of the intermediate microstructure in two-step sintering. Compared to a conventional one-step sintering profile, it significantly improved the sample quality by reducing the grain size and the porosity ratio. At 1200°C (200°C/min) and under 50 MPa, the two-step sintering resulted in Y_2O_3-MgO nanocomposite ceramics with an average grain diameter of about 150 nm (compared to 350 nm with one-step sintering) and a density over 99% (compared to 90% with a one-step sintering). Finally, after post treating the material with HIP at 400 MPa and annealing in air for 100 h, the IR transmission for a thickness of 1 mm exceeds 80% in the IR band II between 3 and 5 µm wavelength. Due to the process, parasitic absorption bands appeared at 3 µm and 7 µm. The first one is in the 3-5 µm range but can be removed by air annealing. The second one is not the the IR band II so for application in that range, it is not a real issue. Moreover, there is almost no opacification at 5 µm up to 500°C and very few up to 1000°C.

The SPS and HIP parameters still need to be optimized, and the processing of bigger parts (up to 100 mm diameter) is under progress.

Funding

This work was supported by the AID (French Innovation Defence Agency) and ONERA (The French Aerospace Lab).

Acknowledgments

The authors would like to thank Frédéric Fossard (ONERA) for the TEM images, Cédric Lopes (ONERA) for HIP post-treatments, as well as Catherine Rio (ONERA), Marie-Hélène Ritti (ONERA) and Katia Dennis (ONERA) for their help during powder processing and characterization of the samples.

References

[1] A. Goldstein et A. Krell, « Transparent Ceramics at 50: Progress Made and Further Prospects », *Journal of the American Ceramic Society*, vol. 99, n° 10, p. 3173-3197, 2016, doi: 10.1111/jace.14553.

[2] D. C. Harris, *Materials for Infrared Windows and Domes: Properties and Performance*. SPIE Press, 1999.

[3] M. E. Thomas, R. I. Joseph, et W. J. Tropf, « Infrared transmission properties of sapphire, spinel, yttria, and ALON as a function of temperature and frequency », *Appl. Opt., AO*, vol. 27, n° 2, p. 239-245, janv. 1988, doi: 10.1364/AO.27.000239.

[4] D. C. Harris, « Durable 3–5 µm transmitting infrared window materials », *Infrared Physics & Technology*, vol. 39, n° 4, p. 185-201, juin 1998, doi: 10.1016/S1350-4495(98)00006-1.

[5] D. C. Harris, « Overview of progress in strengthening sapphire at elevated temperature », in *Window and Dome Technologies and Materials VI*, juill. 1999, vol. 3705, p. 2-11. doi: 10.1117/12.354609.
[6] C. T. Warner, T. M. Hartnett, D. Fisher, et W. Sunne, « Characterization of ALON optical ceramic », in *Window and Dome Technologies and Materials IX*, mai 2005, vol. 5786, p. 95-111. doi: 10.1117/12.607596.
[7] B. H. Kear, R. Sadangi, V. Shukla, T. Stefanik, et R. Gentilman, « Submicron-grained transparent yttria composites », in *Window and Dome Technologies and Materials IX*, mai 2005, vol. 5786, p. 227-233. doi: 10.1117/12.602333.
[8] J. Wang, D. Chen, E. H. Jordan, et M. Gell, « Infrared-Transparent Y2O3–MgO Nanocomposites Using Sol–Gel Combustion Synthesized Powder », *Journal of the American Ceramic Society*, vol. 93, nº 11, p. 3535-3538, 2010, doi: 10.1111/j.1551-2916.2010.04071.x.
[9] D. C. Harris *et al.*, « Properties of an Infrared-Transparent MgO:Y2O3 Nanocomposite », *Journal of the American Ceramic Society*, vol. 96, nº 12, p. 3828-3835, 2013, doi: 10.1111/jace.12589.
[10] D. Jiang et A. K. Mukherjee, « Spark Plasma Sintering of an Infrared-Transparent Y2O3–MgO Nanocomposite », *Journal of the American Ceramic Society*, vol. 93, nº 3, p. 769-773, 2010, doi: 10.1111/j.1551-2916.2009.03444.x.
[11] H. Gleiter, « Nanostructured materials: basic concepts and microstructure », *Acta Materialia*, vol. 48, nº 1, p. 1-29, janv. 2000, doi: 10.1016/S1359-6454(99)00285-2.
[12] S. Xu, J. Li, C. Li, Y. Pan, et J. Guo, « Hot Pressing of Infrared-Transparent Y2O3–MgO Nanocomposites Using Sol–Gel Combustion Synthesized Powders », *Journal of the American Ceramic Society*, vol. 98, nº 3, p. 1019-1026, 2015, doi: 10.1111/jace.13375.
[13] R. Apetz et M. P. B. van Bruggen, « Transparent Alumina: A Light-Scattering Model », *Journal of the American Ceramic Society*, vol. 86, nº 3, p. 480-486, 2003, doi: 10.1111/j.1151-2916.2003.tb03325.x.
[14] A. Krell, T. Hutzler, et J. Klimke, « Transmission physics and consequences for materials selection, manufacturing, and applications », *Journal of the European Ceramic Society*, vol. 29, nº 2, p. 207-221, janv. 2009, doi: 10.1016/j.jeurceramsoc.2008.03.025.
[15] L. Liu, K. Morita, T. S. Suzuki, et B.-N. Kim, « Effect of volume ratio on optical and mechanical properties of Y2O3-MgO composites fabricated by spark-plasma-sintering process », *Journal of the European Ceramic Society*, vol. 41, nº 3, p. 2096-2105, mars 2021, doi: 10.1016/j.jeurceramsoc.2020.10.074.
[16] H. Ryou *et al.*, « Below the Hall–Petch Limit in Nanocrystalline Ceramics », *ACS Nano*, vol. 12, nº 4, p. 3083-3094, avr. 2018, doi: 10.1021/acsnano.7b07380.
[17] L. Liu, K. Morita, T. S. Suzuki, et B.-N. Kim, « Synthesis of highly-infrared transparent Y2O3–MgO nanocomposites by colloidal technique and SPS », *Ceramics International*, vol. 46, nº 9, p. 13669-13676, juin 2020, doi: 10.1016/j.ceramint.2020.02.153.
[18] Z. Shen *et al.*, « Fabrication of infrared-transparent Y2O3–MgO composites using nanopowders synthesized via thermal decomposition », *Ceramics International*, vol. 47, nº 9, p. 13007-13014, mai 2021, doi: 10.1016/j.ceramint.2021.01.164.
[19] C.-H. Chen *et al.*, « A Foaming Esterification Sol–Gel Route for the Synthesis of Magnesia–Yttria Nanocomposites », *Journal of the American Ceramic Society*, vol. 94, nº 2, p. 367-371, 2011, doi: 10.1111/j.1551-2916.2010.04343.x.
[20] H. J. Ma, W. K. Jung, C. Baek, et D. K. Kim, « Influence of microstructure control on optical and mechanical properties of infrared transparent Y2O3-MgO nanocomposite », *Journal of the European Ceramic Society*, vol. 37, nº 15, p. 4902-4911, déc. 2017, doi: 10.1016/j.jeurceramsoc.2017.05.049.
[21] L. Huang, W. Yao, J. Liu, A. K. Mukherjee, et J. M. Schoenung, « Spark plasma sintering and mechanical behavior of magnesia–yttria (50:50vol.%) nanocomposites », *Scripta Materialia*, vol. 75, p. 18-21, mars 2014, doi: 10.1016/j.scriptamat.2013.11.006.
[22] J. Xie, X. Mao, X. Li, B. Jiang, et L. Zhang, « Influence of moisture absorption on the synthesis and properties of Y2O3–MgO nanocomposites », *Ceramics International*, vol. 43, nº 1, Part A, p. 40-44, janv. 2017, doi: 10.1016/j.ceramint.2016.08.117.
[23] Z. Shen *et al.*, « Preparation and study of the mechanical and optical properties of infrared transparent Y2O3–MgO composite ceramics », *Journal of the American Ceramic Society*, vol. 104, nº 12, p. 6335-6344, 2021, doi: 10.1111/jace.18030.
[24] L. Liu, K. Morita, T. S. Suzuki, et B.-N. Kim, « Evolution of microstructure, mechanical, and optical properties of Y2O3-MgO nanocomposites fabricated by high pressure spark plasma sintering », *Journal of the European Ceramic Society*, vol. 40, nº 13, p. 4547-4555, oct. 2020, doi: 10.1016/j.jeurceramsoc.2020.05.046.
[25] L. Dimesso, « Pechini Processes: An Alternate Approach of the Sol-Gel Method, Preparation, Properties, and Applications », in *Handbook of Sol-Gel Science and Technology: Processing, Characterization and Applications*, L. Klein, M. Aparicio, et A. Jitianu, Éd. Cham: Springer International Publishing, 2018, p. 1067-1088. doi: 10.1007/978-3-319-32101-1_123.
[26] S. Ghorbani, R. S. Razavi, M. R. Loghman-Estarki, et A. Alhaji, « Synthesis of MgO-Y2O3 composite nanopowder with a high specific surface area by the Pechini method », *Ceramics International*, vol. 43, nº 1, Part A, p. 345-354, janv. 2017, doi: 10.1016/j.ceramint.2016.09.162.
[27] M.-Y. Chu, L. C. De Jonghe, M. K. F. Lin, et F. J. T. Lin, « Precoarsening to Improve Microstructure and Sintering of Powder Compacts », *Journal of the American Ceramic Society*, vol. 74, nº 11, p. 2902-2911, 1991, doi: 10.1111/j.1151-2916.1991.tb06861.x.
[28] I.-W. Chen et X.-H. Wang, « Sintering dense nanocrystalline ceramics without final-stage grain growth », *Nature*, vol. 404, nº 6774, Art. nº 6774, mars 2000, doi: 10.1038/35004548.

[29] N. J. Lóh, L. Simão, C. A. Faller, A. De Noni, et O. R. K. Montedo, « A review of two-step sintering for ceramics », *Ceramics International*, vol. 42, nº 11, p. 12556-12572, août 2016, doi: 10.1016/j.ceramint.2016.05.065.
[30] H. J. Ma, W. K. Jung, S.-M. Yong, D. H. Choi, et D. K. Kim, « Microstructural freezing of highly NIR transparent Y2O3-MgO nanocomposite via pressure-assisted two-step sintering », *Journal of the European Ceramic Society*, vol. 39, nº 15, p. 4957-4964, déc. 2019, doi: 10.1016/j.jeurceramsoc.2019.07.029.
[31] S. Xu, J. Li, H. Kou, Y. Shi, Y. Pan, et J. Guo, « Spark plasma sintering of Y2O3–MgO composite nanopowder synthesized by the esterification sol–gel route », *Ceramics International*, vol. 41, nº 2, Part B, p. 3312-3317, mars 2015, doi: 10.1016/j.ceramint.2014.10.120.
[32] A. C. Larson et R. B. Von Dreele, « General structure analysis system (GSAS). Technical Report No. LAUR86-748 ». Los Alamos National Laboratory, 2004.
[33] B. H. Toby, « EXPGUI, a graphical user interface for GSAS », *J Appl Cryst*, vol. 34, nº 2, Art. nº 2, avr. 2001, doi: 10.1107/S0021889801002242.
[34] M. I. Mendelson, « Average Grain Size in Polycrystalline Ceramics », *Journal of the American Ceramic Society*, vol. 52, nº 8, p. 443-446, 1969, doi: 10.1111/j.1151-2916.1969.tb11975.x.
[35] S. Deshpande, S. Patil, S. V. Kuchibhatla, et S. Seal, « Size dependency variation in lattice parameter and valency states in nanocrystalline cerium oxide », *Appl. Phys. Lett.*, vol. 87, nº 13, p. 133113, sept. 2005, doi: 10.1063/1.2061873.
[36] S. Sasaki, K. Fujino, et Y. Takéuchi, « X-Ray Determination of Electron-Density Distributions in Oxides, MgO, MnO, CoO, and NiO, and Atomic Scattering Factors of their Constituent Atoms », *Proceedings of the Japan Academy, Series B*, vol. 55, nº 2, p. 43-48, 1979, doi: 10.2183/pjab.55.43.
[37] M. G. Paton et E. N. Maslen, « A refinement of the crystal structure of yttria », *Acta Cryst*, vol. 19, nº 3, Art. nº 3, sept. 1965, doi: 10.1107/S0365110X65003365.
[38] X.-H. Wang, P.-L. Chen, et I.-W. Chen, « Two-Step Sintering of Ceramics with Constant Grain-Size, I. Y2O3 », *Journal of the American Ceramic Society*, vol. 89, nº 2, p. 431-437, 2006, doi: 10.1111/j.1551-2916.2005.00763.x.
[39] S.-M. Yong *et al.*, « Study on carbon contamination and carboxylate group formation in Y2O3-MgO nanocomposites fabricated by spark plasma sintering », *Journal of the European Ceramic Society*, vol. 40, nº 3, p. 847-851, mars 2020, doi: 10.1016/j.jeurceramsoc.2019.10.035.
[40] H. J. Ma, J. H. Kong, et D. K. Kim, « Insight into the scavenger effect of LiF on extinction of a carboxylate group for mid-infrared transparent Y2O3−MgO nanocomposite », *Scripta Materialia*, vol. 187, p. 37-42, oct. 2020, doi: 10.1016/j.scriptamat.2020.05.001.
[41] J. A. Harrington et M. Hass, « Temperature Dependence of Multiphonon Absorption », *Phys. Rev. Lett.*, vol. 31, nº 11, p. 710-714, sept. 1973, doi: 10.1103/PhysRevLett.31.710.